Chemical Transformations of Nanosilver in Biological Environments

Jingyu Liu,[†] Zhongying Wang,[†] Frances D. Liu,[‡] Agnes B. Kane,[§,⊥] and Robert H. Hurt[‡,⊥,*]

[†]Department of Chemistry, [‡]School of Engineering, [§]Department of Pathology and Laboratory Medicine, and [⊥]Institute for Molecular and Nanoscale Innovation, Brown University, Providence, Rhode Island 02912, United States

ABSTRACT The widespread use of silver nanoparticles (Ag-NPs) in consumer and medical products provides strong motivation for a careful assessment of their environmental and human health risks. Recent studies have shown that Ag-NPs released to the natural environment undergo profound chemical transformations that can affect silver bioavailability, toxicity, and risk. Less is known about Ag-NP chemical transformations in biological systems, though the medical literature clearly reports that chronic silver ingestion produces argyrial deposits consisting of silver-, sulfur-, and selenium-containing particulate phases. Here we show that Ag-NPs undergo a rich set of biochemical transformations, including accelerated oxidative dissolution in gastric acid, thiol binding and exchange, photoreduction of thiol- or protein-bound silver to secondary zerovalent Ag-NPs, and rapid reactions between silver surfaces and reduced selenium species. Selenide is also observed to rapidly exchange with sulfide in preformed Ag_2S solid phases. The combined results allow us to propose a conceptual model for Ag-NP transformation pathways in the human body. In this model, argyrial silver deposits are not translocated engineered Ag-NPs, but rather secondary particles formed by partial dissolution in the GI tract followed by ion uptake, systemic circulation as organo-Ag complexes, and immobilization as zerovalent Ag-NPs by photoreduction in light-affected skin regions. The secondary Ag-NPs then undergo detoxifying transformations into sulfides and further into selenides or Se/S mixed phases through exchange reactions. The formation of secondary particles in biological environments implies that Ag-NPs are not only a product of industrial nanotechnology but also have long been present in the human body following exposure to more traditional chemical forms of silver.

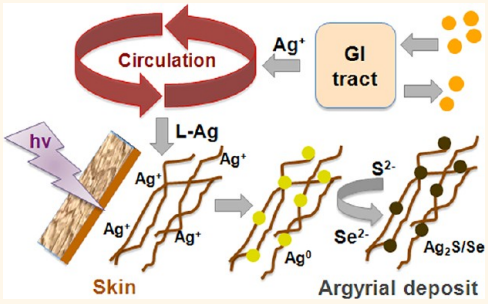

KEYWORDS: silver · selenium · nanomaterial transformation · fate · health risks · photochemistry

Engineered nanomaterials can undergo profound transformation between the time of synthesis and the time at which human or environmental receptors are exposed.[1−4] These material transformations may involve adsorption, chemical reaction, dissolution, or aggregation and can affect transport, bioavailability, bioaccumulation, toxicity, and ultimately risk.

A number of recent studies have focused on the environmental transformations of silver nanoparticles (Ag-NPs).[5−20] These studies show that Ag-NPs undergo slow oxidative dissolution by molecular oxygen and protons,[5,18,19] reactions with reduced sulfur species or chloride,[7,8,10−12,17] adsorption of polymers,[20] natural organic matter (NOM),[15,16,20] or proteins,[21,22] and aggregation that depends on media and coatings.[14,15,17,20,23] The transformed products can show reduced biological activity (*e.g.*, silver sulfide)[24,25] or enhanced biological activity (*e.g.*, the free ion or soluble complexes)[26,27] relative to the initial particle. In the case of silver-based nanomaterials, it has become quite clear that chemical transformations must be considered in any realistic risk assessment.[28,29]

Less is known about Ag-NP transformations in biological systems. The chemical environments in biological systems have some features in common with those in the natural environment (presence of Cl^-, some organic ligands, reduced sulfur species) but also significant differences. Some biological environments have very low pH (gastric fluid), very high concentrations of organic ligands including thiols, significant concentrations of selenium in addition to sulfur, and the potential for photochemistry in the near-skin region. Biological compartments also contain ion channels and pumps, which can transport silver ion by mechanisms evolved in nature for transport of sodium[30] or copper ion.[31] Many aspects of Ag-NP biochemistry are unexplored, such as the interactions with

* Address correspondence to robert_hurt@brown.edu.

Received for review July 31, 2012 and accepted October 9, 2012.

Published online October 09, 2012
10.1021/nn303449n

selenium species, the photochemistry of Ag biocomplexes in the near-skin region, or are incompletely understood, such as the extent of dissolution in the GI tract.[32]

The medical literature does not systematically address the chemical mechanisms and pathways of Ag-NP transformation, but it does provide useful information on the final fate and form of silver in the human body. Overexposure to silver through ingestion, inhalation, and dermal contact can raise silver concentrations in blood and, in some cases, cause irreversible skin discoloration (argyria) especially in sun-exposed areas.[33−46] Silver-rich granules, mostly collocated with sulfur and selenium, have been detected in the connective tissue of the dermis in argyria patients.[33,34,36,41,42,44−46] A recent study reported the deposition of Ag-, S-, and Se-containing nanoparticles in small intestine, liver, and kidney tissue after oral exposure of rats to Ag-NPs.[47] It is clear that a significant long-term fate of silver in the body is as particulate deposits, and the deposition is favored by light exposure, but the chemical pathways have not been systematically investigated and remain unclear.

Here we study the chemical transformations of Ag-NPs in biological media with emphasis on compartments in the human body. We report accelerated dissolution in gastric acid, photoreduction of Ag−thiol and Ag−protein complexes to metallic Ag-NPs, and the ability of reduced selenium species to react with Ag surfaces and to exchange with sulfur on silver surfaces that have been previously sulfidated. The combined results suggest a pathway for argyrial deposits that involves partial gastric digestion to soluble silver, ion uptake, and systematic transport as thiol complexes, photoreduction of Ag(I) to immobilize silver in the form of Ag-NPs in the near-skin region, and then *in situ* transformation to sulfides and selenides. We thus propose that argyrial deposits are *secondary particles* rather than translocated primary particles and, as such, are not unique to Ag-NP exposure but occur upon exposure to a variety of silver compounds and silver-containing materials.

RESULTS

Because of the wide range of nanosilver applications, a variety of exposure routes are relevant including ingestion, inhalation, dermal contact, wound surface application, and insertion or implantation of medical devices.[48] These exposure routes bring Ag-NPs in contact with a range of different fluid environments, and we begin by examining oxidative dissolution at the initial point of entry.

Oxidative Dissolution in Biological Media. Nanosilver is unstable to oxidation and releases ions through gradual reaction with dioxygen and protons or dissolution of pre-existing oxide films in fluid media. Oxidative dissolution is a complex chemical reaction influenced

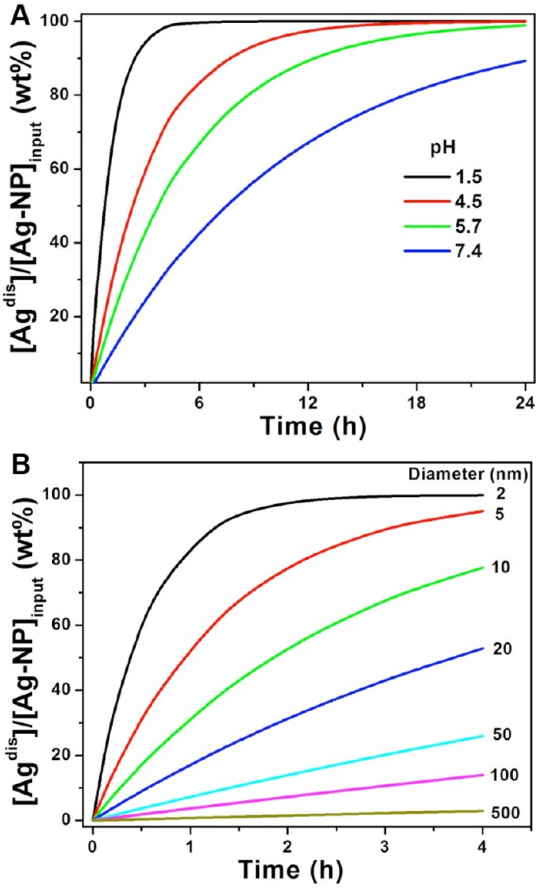

Figure 1. Effects of pH and particle size on Ag-NP oxidative dissolution in simple media estimated using previously published kinetics.[5] (A) pH effect for 5 nm diameter Ag-NPs. (B) Primary particle size effect at pH 1.5. The calculations use the kinetic law of eq 1 at 37 °C and are reported as cumulative wt % of total input silver released as ions.

by pH, coatings, and ligands in the surrounding fluid[5,6,8,11,12,14,16,18,26,49] and has been extensively characterized in environmental fluid phases,[5,11,12,14,16,49] but less so in biological media,[6,11,50] though the important role of released silver ions in Ag-NP toxicity is well-recognized.[26,27,51,52] Biological compartments cover a wide pH range (1−8), and we expect pH[5,19] and particle surface area (particle size and aggregation state)[6,18,19,27,52,53] to be important factors influencing biodissolution rates. Figure 1 explores the effects of pH and primary particle size in four media representing the (1) stomach (pH 1.5),[54] (2) lysosome (pH 4.5),[55] (3) inflammatory phase of acute wounds (pH 5.7),[56] and (4) extracellular environment/blood/lung fluid (pH 7.4),[54] using previously published kinetics for a model citrate-capped Ag-NP material system:[5]

$$-\frac{1}{m}\frac{dm}{dt} = Ae^{-E/RT}\left(\frac{[H^+]}{10^{-7}\mathrm{M}}\right)^n \qquad (1)$$

where $E = 77$ kJ/mol, $A = 2.5 \times 10^{13}$ day^{-1}, and $n = 0.18$. An area normalized form useful for estimating the size dependence has $(1/S)(-dm/dt)$ on the left-hand side

and a pre-exponential factor $A = 7.6 \times 10^{16}$ μg release/day·m^2·particle surface. Figure 1 suggests that the low pH in gastric fluid will lead to accelerated dissolution of Ag-NPs in the stomach, but that dissolution will be incomplete for most particles due to limited residence time (10−240 min in stomach).[57] Ligand, coating, and salt effects limit our ability to accurately predict dissolution rates in complex media at this time from simple approaches such as the use of eq 1, so experimental data on gastric fluid and wound fluid simulants are needed to confirm this conclusion. Our previous work used ultrafiltration/atomic adsorption (AA) for release rate measurement, which is quantitative but incompatible with the presence of proteins or other macromolecules, which can bind Ag^+ and be removed by the ultrafilter, leading to incorrect assignment of Ag to the condensed (particle) phase. At high silver doses (above those relevant to the natural environment), $AgCl_{(s)}$ may also form and be removed by ultrafiltration, and chloride has been reported to cause matrix effects that interfere with the atomic absorption method.[58] For experiments in biological media, therefore, we need an alternative technique and chose to adapt an *in situ* plasmon resonance tracking method.[11,59]

Ag-NPs are well-known to exhibit strong localized surface plasmon resonance (LSPR), and the corresponding UV−vis absorption peak is sensitive to particle size, shape, aggregation state, and the external dielectric environment[60] and can be used to monitor total Ag concentration.[59,61] We adapted the technique of Espinoza[59] and Zook[11] with modification by using 1 wt % polyvinylpyrrolidone (PVP) to protect particles from aggregation and UV−vis absorbance to track ion release. The technique was first validated by oxidatively dissolving Ag-NPs in 0.084 M HNO_3, which gives the same pH as synthetic gastric acid. Figure 2A shows a rapid decrease of the LSPR signal at ~397 nm, corresponding to Ag^0 oxidation. Assuming that optical absorption at the LSPR peak height is proportional to total Ag^0 concentration[59] gives a release curve that can be compared to direct measurement by ultrafiltration/AA (Figure 2B). Figure 2B validates the LSPR technique, which can now be used in complex media containing Ag-binding macromolecules that cannot pass the ultrafilter (MW cutoff 3K).

Figure 3 uses the LSPR technique to measure silver ion release profiles in gastric fluid and pseudoextracellular fluid (PECF) with BSA as a simulant for wound exudate. Dissolution is relatively rapid in gastric fluid in agreement with the behavior in simple media (dashed black curve) and is very slow in PECF. The elevated pH in PECF is not sufficient to explain the slow dissolution (see dashed red curve) and may be related to ligands in the PECF buffer. Interestingly, the presence of albumin greatly accelerates ion release. It is possible that the strong affinity of BSA for Ag^+[62] facilitates the mobilization of surface-bound Ag^+ to the solution phase,

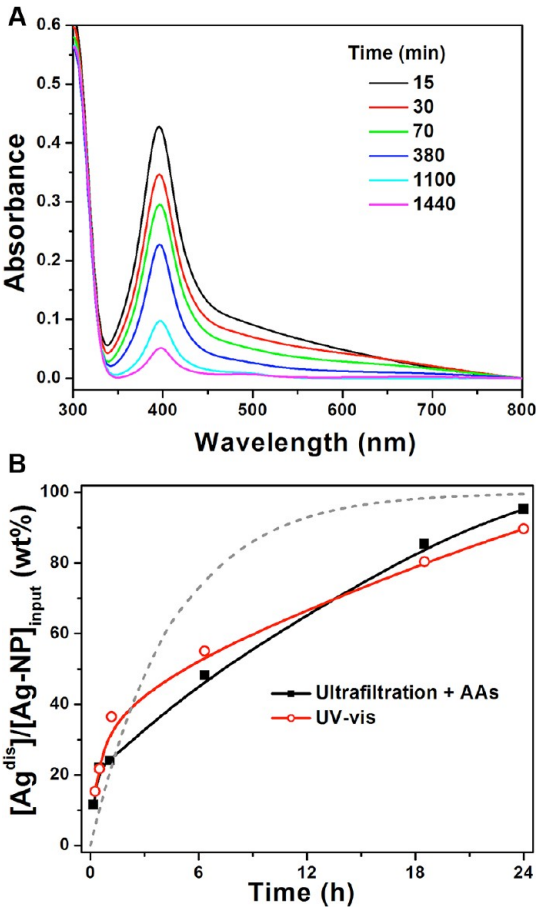

Figure 2. Development and validation of plasmon resonance tracking technique for Ag-NP (average diameter 5 nm) dissolution in complex media. (A) UV−vis spectra recorded during incubation of Ag-NP in dilute HNO_3, showing rapid decrease of peak absorbance due to oxidative dissolution. (B) Comparison of time-resolved Ag-NP dissolution measured by UV−vis and ultrafiltration/AA, demonstrating UV−vis as an alternative tool for quantifying silver ion release. The gray dashed curve gives calculated release kinetics at pH 1.1 using eq 1. The release experiment was conducted using Ag-NP suspension (initial concentration 5 mg/L) in 0.084 M HNO_3 supplemented with 1 wt % PVP at room temperature in the dark.

though more work is needed to understand this phenomenon.

Interaction of Ag^+ with Chloride and Thiol. The Ag^+ produced by oxidative dissolution can further transform in biological media, whose composition determines the speciation, mobility, and bioactivity of silver. The free Ag^+ concentration in biological media is extremely low due to complexation and possibly precipitation of Ag^+ with Cl^-, typically on the order of 10^{-9} M ($K_{sp} = 1.77 \times 10^{-10}$ for AgCl).[65] The maximum concentration of soluble silver species (sum of Ag^+, $AgCl_{(aq)}$, $AgCl_2^-$, and $AgCl_3^{2-}$) estimated using visual MINTEQ (version 3.0)[66] is 0.51 and 0.58 mg/L in synthetic gastric acid and albumin-free wound simulant, respectively. Above this concentration, $AgCl_{(s)}$ will appear and limit further increases in silver bioavailability.[67] In many exposure scenarios, the total silver

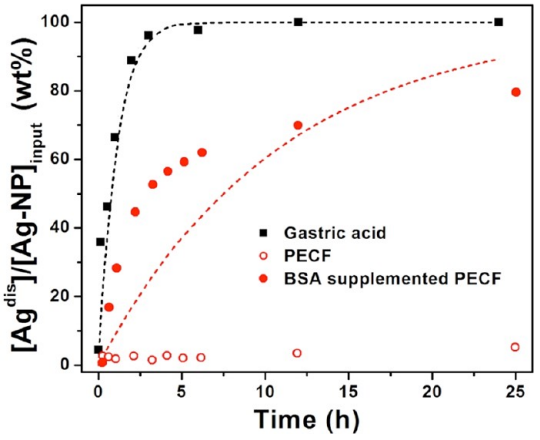

Figure 3. Time-resolved silver ion release from Ag-NPs (average diameter 5 nm) in synthetic gastric fluid (pH 1.12) and wound fluid (pH 7.52). The black and red dashed lines represent the calculated silver ion release in simple media pH 1.5 and 7.4 buffer, respectively. The release experiments were conducted using initial Ag-NP concentration of 5 mg/L in simulant biological media at 37 °C in the dark. The PECF[63] and PECF supplemented with 20 mg/mL BSA[64] were used to mimic wound exudate. At each time point, a 300−800 nm UV−vis spectrum was recorded and the absorbance at 397 nm was used to determine total elemental silver.

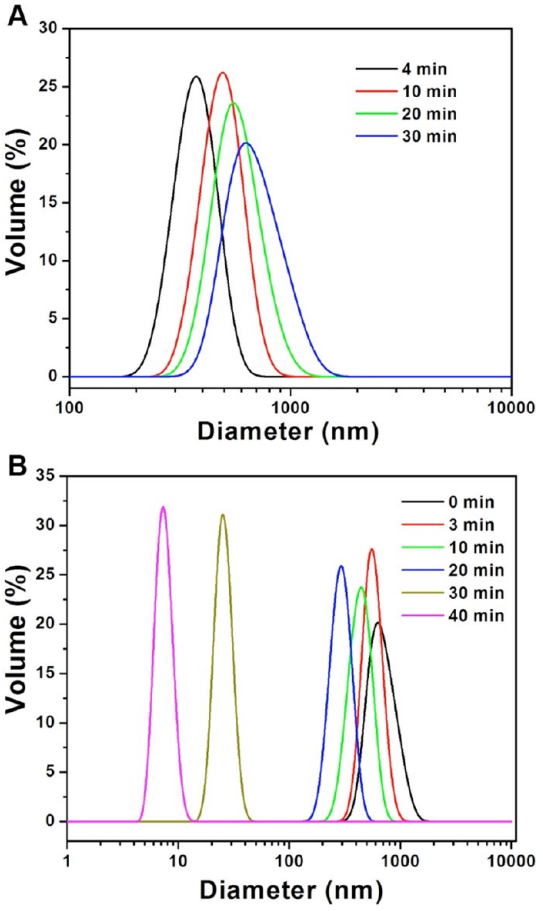

Figure 4. Demonstration of Ag^+ interactions with chloride and preferred binding to thiol. (A) Time-resolved measurement of hydrodynamic particle sizes during formation and growth of AgCl particles upon addition of $AgNO_3$ into PBS buffer. (B) Further time-resolved hydrodynamic particle size measurement showing $AgCl_{(s)}$ decomposition upon addition of the small molecule thiol, glutathione (GSH). One millimolar $AgNO_3$ was mixed with PBS buffer for 30 min, followed by addition of 1 mM GSH. The DLS signal disappears after 45 min, indicating complete dissolution of $AgCl_{(s)}$.

dose is less than these values (<0.5 ppm), so $AgCl_{(s)}$ is not expected as a product, but it can occur at high doses and especially in toxicity studies, where elevated doses are used to produce acute effects.[68,69]

The Ag^+ and its soluble complexes in the GI tract can be taken up into systemic circulation by active transport routes for Na^+ and Cu^+[70] and enter the bloodstream, where it is expected to bind to proteins and distributed to a variety of tissues and organs.[71] Serum albumin, the most abundant plasma protein, is involved in the transport of other ions including Cu^{2+}, Ni^{2+}, Zn^{2+}, and Co^{2+}.[72−75] The affinity of human serum albumin (HSA) toward Ag^+ and the abundance of HSA in blood (50 g/L)[76] make serum albumin a likely transporter for Ag^+. Binding sites for Ag^+ on HSA have been reported with the formation constants of 10^5 and 10^4, and cysteine, methionine, and disulfide bridge residues are the major functional groups involved.[77] In general, the soft acid Ag^+ binds strongly to thiol (−SH) groups (log $K_{formation}$ = 11.9 for Ag^+-cysteine)[78] including small molecule thiols such as reduced glutathione (GSH).[79] GSH is a primary endogenous antioxidant with a typical blood concentration of 1 mM.[80] Here we use GSH as a model thiol compound to investigate Ag^+ binding, exchange, and competition with chloride species in biological fluids.

We first observed that free Ag^+ and free GSH show no coexistence region in DI water (Supporting Information, Figure S1) consistent with the strong binding reaction: $Ag^+ + GSH \leftrightarrow GS\text{-}Ag + H^+$.[81] At high GSH/Ag ratio, the stoichiometry of the complex is Ag-GSH, while at low ratios, the stoichiometry approaches Ag_2-GSH. The removal of reaction products using centrifugal ultrafiltration (MW cutoff 3K) indicates the formation of high molecular weight silver−GSH polymer complexes. Silver−thiol polymers were reported to have a two-dimensional layered structure with Ag−S bonds in a three-coordinate mode,[82] and silver-rich complexes were also identified where excess silver binds to sulfur groups or forms Ag−Ag bonds with mercaptide-bound silver atoms.[83,84] More information on silver−thiol polymers is found in the Supporting Information.

An important question for biological partitioning is whether Ag^+ can exchange easily between high affinity ligands such as Cl^- and RSH and remain mobile. To test chloride/thiol exchange, we first formed AgCl precipitates and exposed them to GSH while tracking particle size by dynamic light scattering (DLS). Figure 4A shows that addition of $AgNO_3$ to PBS buffer causes rapid precipitation of AgCl, and the particle

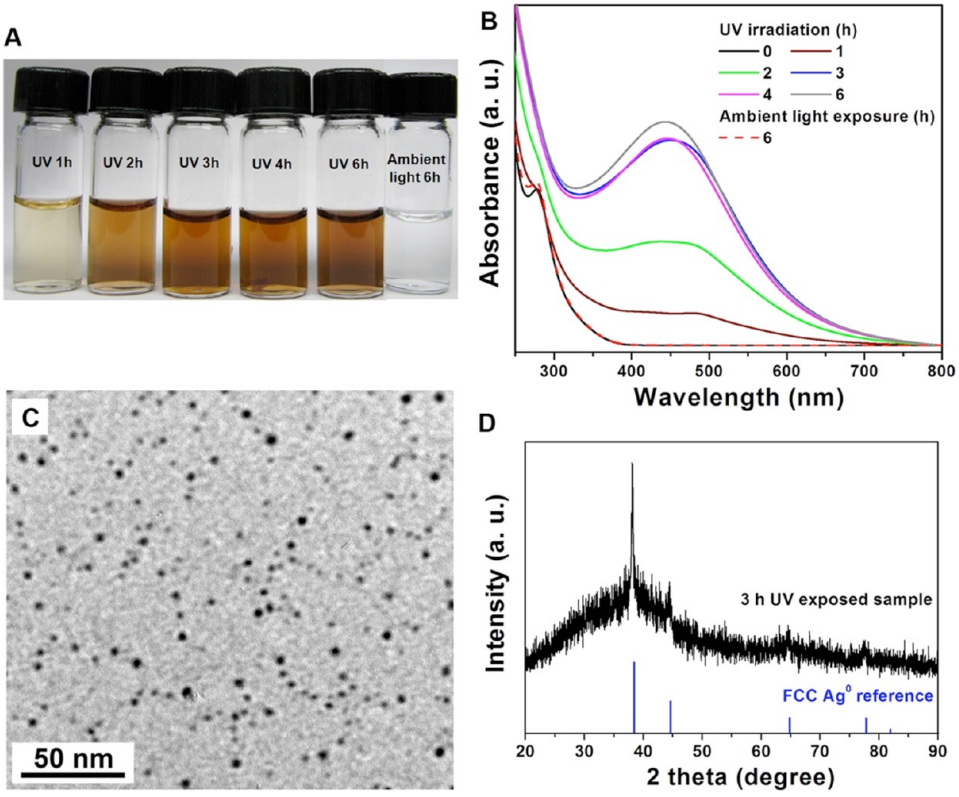

Figure 5. UV irradiation induces Ag-NP formation in $AgNO_3$/GSH mixtures at concentration ratio of 1/0.3 in DI water. (A) Photographs after 1−6 h light exposure show nanoparticle formation only at UV wavelengths. (B) UV−vis spectra of samples in (A). (C) TEM image of 3 h UV-exposed sample, confirming the generation of nanoparticles. (D) Identification of product phase by XRD. Experiments were conducted by exposure of 5 mL of $AgNO_3$ (1 mM) and GSH (0.3 mM) mixture to UV light (365 nm) or ambient lab light.

size increases quickly from ~300 nm to micrometers. Addition of GSH (Figure 4B) dissolves the AgCl precipitates within 45 min to produce Ag-GSH complexes that can be monomers or soluble oligomers undetectable by DLS. We note that silver−GSH complexes have been shown to be bioavailable to aquatic organism[85] and were reported to enhance silver transport from AgCl across simulated biological membranes.[86] Silver is also reported to readily exchange between different thiol groups[87] despite the strong Ag−thiol bond. Well-dispersed silver−GSH complexes are likely important transporters that deliver silver to biological targets through thiolate ligand exchange.[87] By this mechanism, silver can be transported and distributed across multiple tissue and organ systems following systematic absorption.[71] Of special interest here are clinical cases of argyria where silver is located in the basement membrane of skin as particles,[34,36,38,41,42,44] with an unknown formation mechanism.

Biological Photochemistry of Silver. Argyria, characterized by the irreversible bluish-gray discoloration of skin, is most prominent in light-affected skin areas and has been characterized as a particulate phase with Ag collocated with S and/or Se.[34,36,38,41,42,44,45] The clinical pattern of sunlight dependence suggests the importance of a photocatalyzed reaction. Here we start with the silver−thiol and silver−protein complexes described in the previous section and study their behavior under UV−visible light.

Figure 5A shows that clear silver−GSH complexes in DI water gradually darken over 6 h under 365 nm UV irradiation but not in room light. Figure 5B shows full spectra, which develop a broad 400−550 nm band over time under UV irradiation but not in room light. TEM (Figure 5C and Figure S2) and XRD (Figure 5D) show that this process is accompanied by nanoparticle formation in face-centered cubic (fcc) Ag^0 phase. Similar phototransformations were also observed in PBS buffer (Figure 6) and in selected experiments using different GSH/Ag^+ ratios or using cysteine and oxidized glutathione (GSSG) as thiol sources. In each case, the product was zerovalent nanosilver (Supporting Information, Figure S3). Note that prolonged incubation of $AgNO_3$/GSH for several days in room light or dark causes a similar color change to that in Figure 5, which must be uncatalyzed GSH reduction[88] such as may occur in dark deep tissues, but more slowly.

It is clear that UV irradiation of Ag complexes with small molecule thiols produces Ag-NPs. Much of the thiol content in blood and tissue is found in protein, and the main component of basement membrane connective tissue, where argyrial deposits are often

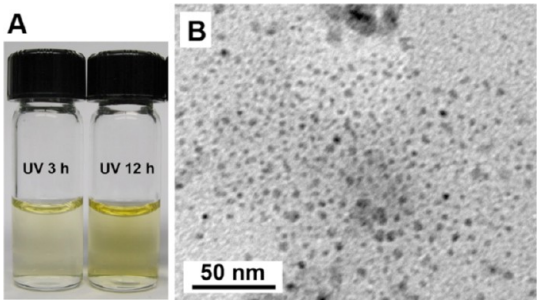

Figure 6. UV irradiation induces formation of small-diameter Ag-NPs from $AgNO_3$/GSH mixtures at a concentration ratio of 1/1 in PBS buffer. (A) Photograph of the mixture after exposed to UV for 3 and 12 h. (B) TEM image of 12 h UV-exposed sample in (A). Experiments were conducted by exposure of 5 mL of $AgNO_3$ (1 mM) and GSH (1 mM) mixture in PBS buffer under UV light (365 nm).

found, is the protein collagen. Here we exposed type I collagen solutions to $AgNO_3$ and UV and observed irregularly shaped silver nanostructures (Figure 7A,B). SAED pattern identifies the phase again as polycrystalline fcc Ag^0 (Figure 7B). Figure 7C gives UV−vis spectra, showing that photoreduction progresses over time and even occurs to some extent under room light. Photoreduction of $AgNO_3$ in collagen solution is fast—the fraction of input Ag^+ that is reduced increases from 30 to 50% between 1 and 5 h exposures (Figure 7D). Experiments using a gel form of collagen that more closely mimics the physical form of tissue also provide evidence of Ag-NP formation under UV−vis light with no transformation in the dark (Supporting Information, Figure S4).

Together, these data show that a range of thiol-containing biomolecules and proteins produce zerovalent Ag-NPs upon UV photodecomposition with slower rates in visible light. The chemistry demonstrated here is related to that in black-and-white photography and in biological silver staining.[89] Because these decomposition products are zerovalent Ag rather than sulfide phases, the photodecomposition alone is not a sufficient explanation for the known composition of argyrial deposits and an additional mechanism is needed (next section).

Sulfide and Selenide Reactions. We thought originally that Ag/S/Se argyrial particles may come directly from Ag−thiol/selenol photodecomposition, but the data show that the photodecomposition products are not sulfides but zerovalent Ag particles. It has been established that Ag_2S-NPs can be generated by direct sulfidation of such Ag-NPs under conditions relevant to the natural environment.[7−10] Sulfides are present in the human body at concentrations reported from the nanomolar range[90] up to 10−100 μM,[91] and the corresponding sulfidation time scales range from hours to days,[7] making Ag-NP sulfidation a plausible transformation in biological systems as it is in the natural environment. Because previous literature has focused on Ag-NP sulfidation reactions, we focus here on Ag-NP reactions with selenium, which are unique to the biological setting.

The pathways leading to colocalization of Ag and Se in argyrial deposits were initially unclear. We found no literature on Ag/Se biochemistry, although selenium reactions with silver nanoclusters are the basis for the "selenium toning" technique used for stylistic and stability enhancement in black-and-white photography.[92] We designed experiments to see if selenium can "tarnish" silver surfaces in a manner similar to sulfur.[7] Because selenide oxidizes more readily than sulfide, we used selenite (SeO_3^{2-}) and $NaBH_4$ to generate reduced selenium (Se^{x-}, $x = 1$ or 2) *in situ*[93] in anaerobic atmospheres in a glovebox (with continuous measurement of O_2 at <0.2 ppm). Addition of silver foil to this solution leads to visible tarnish within 30 min, and the XRD spectrum after 1 week shows the formation of crystalline silver selenide (Figure 8). The route to Ag_2Se may run through Se^{2-} and trace O_2 in analogy to oxysulfidation.[7] More likely at this low oxygen content is partial reduction of selenite by sodium borohydride to diselenide[94] followed by disproportionation to Ag_2Se and Se^0. We do observe the characteristic red nanoparticles of Se^0 as a byproduct in some experiments. Both selenide and diselenide are important intermediates in human selenium metabolism.[95]

The much lower abundance of Se in the human body relative to S (~1/10 000)[96,97] makes it unlikely that selenium could compete kinetically with sulfur in its reaction with silver surfaces. This kinetic advantage suggests initial formation of silver sulfides, but this would require another separate mechanism to explain the incorporation of Se in argyrial deposits. Silver sulfide is highly insoluble ($K_{sp} = 5.92 \times 10^{-51}$ for Ag_2S)[28] but silver selenide even more so ($K_{sp} = 3.1 \times 10^{-65}$ for Ag_2Se),[98] which makes the replacement reaction thermodynamically favorable:

$$Ag_2S + Se^{2-} \leftrightarrow Ag_2Se + S^{2-}$$
$$\Delta G^0_{rxn} = -81.5 \text{ kJ/mol} \quad (2)$$

One might expect that the very low solubility of Ag_2S would make this reaction slow unless it proceeds through a solid-state mechanism. We were unable to find data on the extent or mechanisms of Se incorporation into Ag/S phases to evaluate the possibility of this exchange reaction. We therefore conducted experiments in which Ag_2S surfaces were created and exposed to selenide generated *in situ*. The Se/S exchange reaction with sulfidated silver foils was readily observed: within 1 day, selenium replaces sulfur on S-tarnished silver films as determined by EDS (Table S1, Supporting Information). The exchange reaction was studied in detail for Ag_2S nanoparticles by presulfidating Ag-NPs and incubating them in reduced selenium solutions at equal Se/S molar ratios. The XRD spectra in Figure 9 show that the Se/S exchange reaction is complete after 3 days and the final product

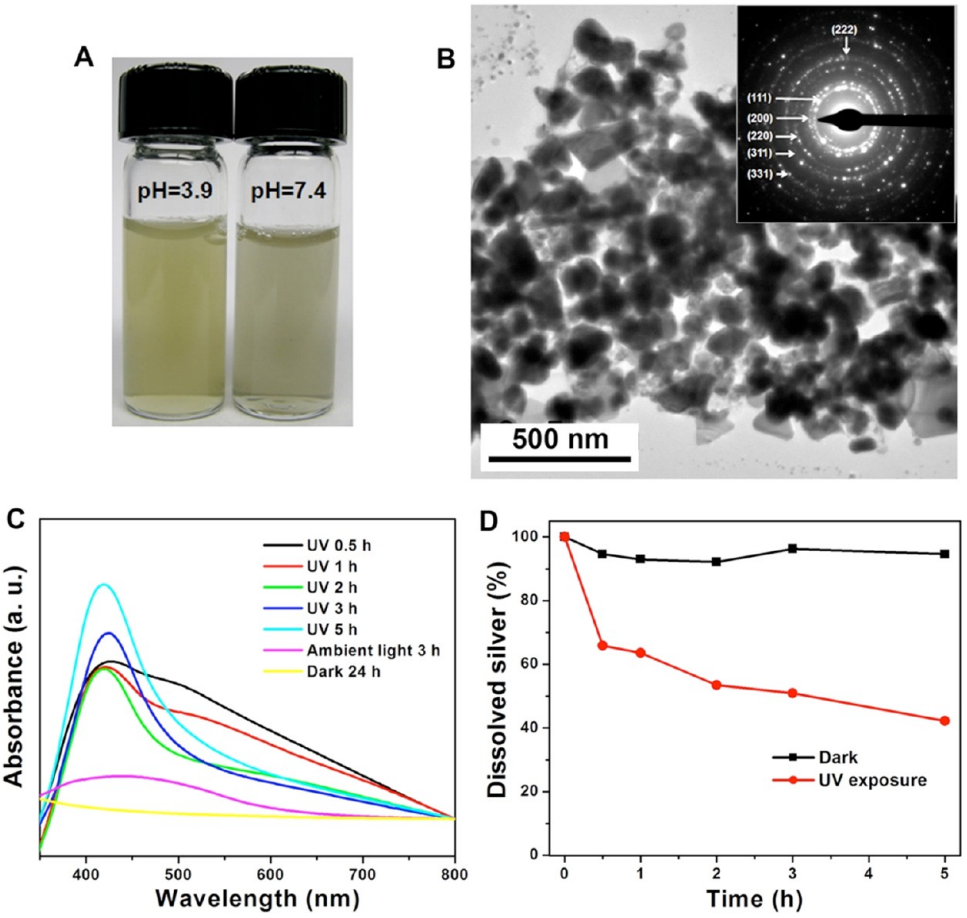

Figure 7. Photoreduction produces Ag-NPs in collagen solutions. (A) Photograph of $AgNO_3$ (1 mM) in collagen solution (0.1 mg/mL) at pH 3.9 and 7.4 after UV irradiation for 3 h. (B) TEM image of 3 h UV-exposed sample at pH 7.4; the inset gives SAED pattern corresponding to fcc Ag^0. (C) UV−vis spectra of sample solutions under various exposure conditions. (D) Dissolved silver measurement in sample solutions during dark or UV-irradiated incubation, showing that photoreduction only occurs under UV exposure. Experiments were conducted by exposure of 5 mL of $AgNO_3$ (1 mM) and 0.1 mg/mL collagen mixture at pH 3.9 (A) or pH 7.4 (A−D) under UV light (365 nm). The collagen working solution diluted from vendor's stock gave a pH of 3.9 and was adjusted to pH 7.4 with NaOH. The dissolved silver concentrations were quantified using AA after removal of Ag-NPs by centrifugal ultrafiltration.

is Ag_2Se with no detectable Ag_2S. The preference of Ag(I) for Se over S is both thermodynamically predicted and observed in experiment, and the exchange reaction goes to completion over times easily accessible in laboratory studies.

SUMMARY AND CONCLUSIONS

The goal of this study was to investigate the chemical pathways for Ag-NP transformation in biological media relevant to human exposures. Our results show accelerated oxidative dissolution in the GI tract, preferential thiol binding and exchange reactions, photodecomposition of Ag biocomplexes to zerovalent Ag-NPs, and reactions with sulfur and selenium. Particularly interesting findings are the selenium tarnishing of silver surfaces and the ability of selenide to rapidly replace sulfide in Ag_2S-NPs and Ag_2S films through exchange reaction.

Of particular interest in this study were the chemical pathways leading to argyria. The medical literature provides multiple case studies that document argyrial deposits as Ag/S/Se particulate phases located in the near-skin region, and that deposition occurs preferentially in light-affected regions. The combined results of the present study allow us to propose a conceptual model for argyrial pathways (Figure 10). Ingestion or inhalation followed by macrophage clearance can bring Ag-NPs into the GI tract. The very low pH in the stomach leads to ion release, but the short residence time should cause the extent of dissolution to be incomplete in many cases. Silver ion and its complexes are brought into the bloodstream through ion or nutrient uptake channels and circulate systematically. Note that NPs can also enter the body directly through wounds, implants, damaged skin, lung translocation, or through GI tract, but the ability of particles to cross the gut epithelium is limited,[99] and in this case, ion uptake is likely the main route to systemic circulation (*vida infra*).

The majority of silver in circulation is predicted to be bound to thiol complexes, which have high binding

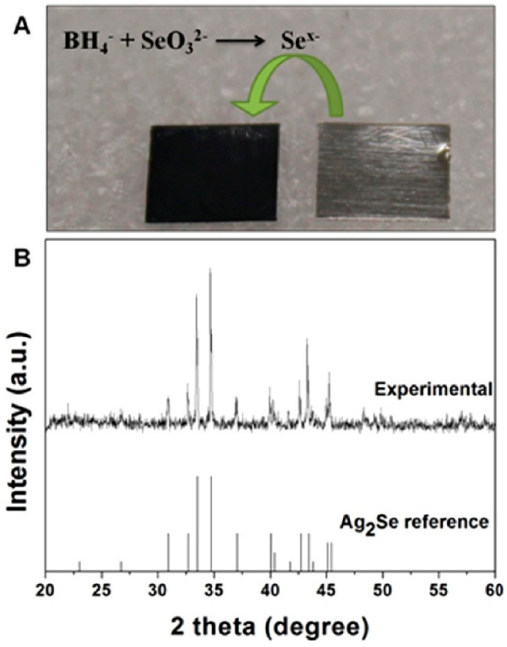

Figure 8. "Tarnishing" of metallic silver foil with reduced selenium species generated *in situ* in aqueous media. (A) Optical image of silver foil (99.9% Ag) incubated with DI water (right) and reduced selenium (left) for 7 days, showing black scale formation only in presence of reduced selenium. (B) XRD spectra of 7 day sampling, indicating formation of crystalline Ag_2Se. Experiments were performed in low-oxygen atmospheres for stability with Se^{x-} (x = 1 or 2) species ([selenium] = 5 mM) generated *in situ* by $NaBH_4$ reduction of Na_2SeO_3.

affinities but are easily exchangable, giving Ag(I) a significant biomolecular mobility. (We note that sulfides and selenides have even higher binding affinities than thiols but are orders of magnitude lower in concentration in physiological fluids, so binding kinetics strongly favor complexation of silver to thiol as a first step in the pathway.) The Ag(I) that reaches the near-skin region in light-affected areas can be easily photoreduced to metallic Ag-NPs, which effectively immobilizes the silver. The immobilization is both physical, due to low particle diffusivity, and chemical since the thiol exchange reactions of Ag(I) are not possible with Ag(0). Once formed, the Ag-NPs transform to sulfide phases in analogy to the documented environmental transformations.[7−10] Possibly unique to biological systems is the incorporation of selenium. The low concentrations of selenium relative to sulfur make it difficult for selenium to compete kinetically with sulfur, but over longer times, the higher affinity of Se for Ag (lower K_{sp}, free energy) predicts selenides as the equilibrium state. Our results demonstrate for the first time the ability of selenide to exchange with sulfide in silver phases, giving a plausible route for the known formation of biological silver selenides in argyrial deposits. Both the sulfide and selenide transformations can be regarded as biological detoxification reactions due to the low bioavailability of silver in the highly insoluble products.

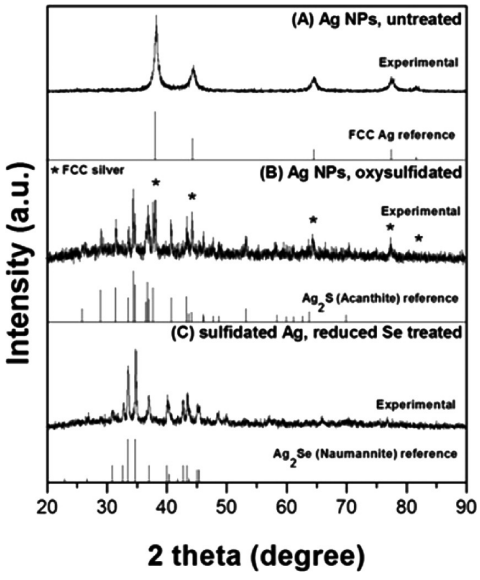

Figure 9. Demonstration of Se/S exchange reactions in Ag-containing nanoparticles. (A) XRD pattern of pristine silver nanopowder (20−40 nm, QuantumSphere), giving fcc metallic silver. (B) XRD spectrum of sulfidation product, showing conversion to acanthite Ag_2S phase with some residual Ag^0 (star labeled peaks). Experiment was conducted by incubating silver nanopowder (10 mM) in Na_2S (5 mM) for 3 days in air-saturated water. (C) XRD spectrum of sulfidation product exposed to reduced selenium species, confirming the exchange reaction from Ag_2S to Ag_2Se. Sample was prepared by incubating presulfidated silver nanopowder (5 mM) in reduced selenium generated *in situ* from Na_2SeO_3 (5 mM) with $NaBH_4$ (25 mM) in an anaerobic atmosphere (O_2 ~0.1 ppm) for 3 days.

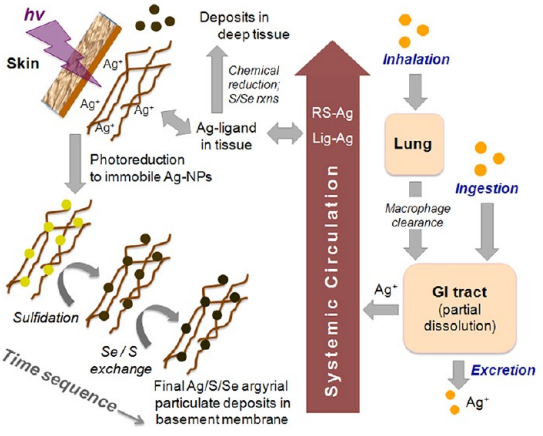

Figure 10. Summary of the biological transformations of Ag-NPs and conceptual model for formation of argyrial deposits. The Ag/S/Se argyrial particulate is proposed to be the result of gastric dissolution, ion uptake, circulatory thiol transport, and photoreduction to immobile secondary particles of zerovalent silver followed by sulfidation and Se/S exchange reactions. Ag^+ complexes may be secondarily reduced in deep tissues at slower rates by nonphotochemical processes.

One implication of these results is that argyrial deposits are primarily secondary particles rather than translocated primary particles. As such, they are not unique to Ag-NP exposure but occur upon exposure to a variety of silver compounds and silver-containing

TABLE 1. Synthetic Biological Fluids

simulant fluids	components	pH
gastric acid[106]	2 g/L NaCl, 7 mL/L 37% HCl	1.12
pseudoextracellular fluid[63]	6.8 g/L NaCl, 2.2 g/L KCl, 25 g/L $NaHCO_3$, 3.5 g/L KH_2PO_4	7.52
BSA-supplemented pseudoextracellular fluid[64]	6.8 g/L NaCl, 2.2 g/L KCl, 25 g/L $NaHCO_3$, 3.5 g/L KH_2PO_4, 20 g/L BSA	7.52

materials. This secondary particle idea and the proposed dissolution−complexation−photoreduction−sulfidation/selenation pathway in Figure 10 is consistent with the observed fact that some argyrial cases occur in patients who have ingested silver forms that do not appear to contain particles.[33,34,100−102] Particularly relevant support for our proposed pathway is found in a recent article in this journal,[102] in which rats were orally exposed to either soluble silver or two different silver nanoparticles. The biodistribution patterns were observed to be similar for soluble and NP forms, and particles were observed in tissue even when the rats were only fed soluble (nonparticulate) silver. The authors conclude that the particles in tissue must be formed *in vivo*, and that the combined evidence suggests that ionic silver is the main bioavailable form following oral ingestion of silver salts or silver NPs.[102]

The spontaneous formation of silver-containing nanoparticles in this and other studies[103−105] remind us that Ag-NPs not only are the product of industrial nanotechnology but also may form spontaneously in environmental or biological systems following exposure to other more traditional chemical forms of silver.

MATERIALS AND METHODS

Materials. Citrate-stabilized Ag-NPs with average diameter of 4−5 nm were synthesized by borohydride reduction.[5] Typically, a 59.2 mL solution containing trisodium citrate (0.6 mM) and $NaBH_4$ (2 mM) was prepared in DI water (Millipore, 18.3 MΩ·cm). While being vigorously stirred in an ice bath, a 0.8 mL solution of 15 mM $AgClO_4$ was quickly added into the mixture followed by 3 h additional stirring. The resulting brownish yellow Ag-NP suspension was purified with 2 cycle DI water wash using centrifugal ultrafiltration (Amicon Ultra-15 3K, Millipore, MA), concentrated to ∼40 mg/L, and stored at 4 °C in the dark for later use. Silver nanopowder (average diameter 20−40 nm) manufactured by a vapor condensation process (QuantumSphrere, CA, USA) and silver foil (Strem Chemicals, MA, USA; 99.9% Ag, 0.127 mm thickness) were used as reference silver materials. Type I collagen (10.12 mg/mL in 0.02 M acetic acid) from rat tail tendon was purchased from BD Biosciences (NJ, USA), and 10× phosphate buffered saline (PBS) was obtained from Fisher Scientific (MA, USA) and diluted with DI water to 1× concentration before use. ThioGlo-1, a maleimide reagent used as fluorescent probe for measuring GSH concentration, was purchased from Calbiochem, Inc. (CA, USA).

Ag-NP Oxidative Dissolution in Simulated Biological Media. Ag-NP oxidative dissolution experiments were conducted in synthetic gastric acid and wound fluids. The chemical compositions of the media are listed in Table 1. Pseudoextracellular fluid (PECF) and BSA-supplemented PECF were used to simulate wound exudates.[63,64] A solution containing 10 mg/L Ag-NPs and 2 wt % PVP was first prepared by adding fresh PVP solution (10 wt %) into citrate-stabilized Ag-NP stock suspension; after incubation at 4 °C for 5 min, this solution was mixed with equal volume of 2× concentrated synthetic biological fluids to produce testing solution with a Ag-NP concentration of 5 mg/L and PVP concentration of 1 wt %. The Ag-NP suspensions were then incubated at 37 °C in the dark for up to 24 h, during which period silver ion release was monitored by measuring the localized surface plasmon resonance (LSPR) absorbance using UV−vis spectrometry. Typically, an aliquot of Ag-NP suspension was taken during incubation, and the UV−vis spectra were recorded between 300 and 800 nm on a V-630 spectrophotometer (Jasco, MD) using particle-free media as background. The peak shift was negligible (<5 nm) over the course of the experiment, indicating that PVP successfully protects particles from aggregation. The Ag-NP suspension gives a LSPR peak at ∼397 nm, and the absorbance is given by Beer's law, $A = \varepsilon lc$, where ε is the absorptivity, l is the path length, and c is Ag^0 concentration. The mass percentage of Ag-NP dissolution can be derived by

$$[Ag^{dis}]/[Ag\text{-}NP]_{input} = (A_0 - A_t)/A_0 \times 100\% \quad (3)$$

Control experiments using Ag-NP dissolution in HNO_3 were performed to validate this method. A test solution containing 5 mg/L Ag-NP and 1 wt % PVP was prepared in 0.084 M HNO_3 (the same proton concentration as in synthetic gastric acid). During incubation in the dark at room temperature, silver ion dissolution was quantified with both LSPR absorbance-based method as described above or graphite furnace atomic absorption spectrometry (AA) (PerkinElmer AAnalyst 600) after removal of Ag-NPs using centrifugal ultrafiltration (Amicon Ultra-15, 3K).

Silver−Glutathione Complex Formation. The stoichiometry of silver−GSH complex formation was measured by tracking the concentration change of $AgNO_3$ and GSH using AA and ThioGlo-1 fluorescence assay, respectively. A kinetic experiment was first performed by mixing $AgNO_3$ and GSH both at final concentration of 1 mM in DI water, followed with quantification of soluble silver using AA after collection of aqueous phase by centrifugal ultrafiltration. On the basis of the rapid reaction kinetics, 30 min was used for the dose-dependent experiments. Typically, the final $AgNO_3$ concentration was fixed at 1 mM, and GSH was added into $AgNO_3$ at a concentration of 0.1 to 4 mM; after incubation in the dark at room temperature for 30 min, the aqueous phase was isolated with ultrafiltration filter. An aliquot of the filtrate was analyzed by AA for soluble silver concentration, and another aliquot was used to measure the GSH concentration using ThioGlo-1 fluorescence reagent.[107] Details on the fluorescence assay are provided in Supporting Information.

The decomposition of AgCl precipitate by GSH was studied in PBS buffer. $AgNO_3$ was first added into PBS buffer at 1 mM, and the immediate formation and growth of AgCl precipitates were monitored using dynamic light scattering (DLS) on a Zetasizer Nano ZS system (Malvern Instruments). After 30 min, GSH was added into the AgCl precipitate at 1 mM, the white precipitate gradually disappeared, and the hydrodynamic size of the decomposed particles was tracked with DLS for up to 1 h.

Photodecomposition of Silver Complexes. The further transformation of silver after dissolution and complex formation was investigated by exposure of various test solutions containing 1 mM $AgNO_3$ to UV light. The thiol (−SH) or disulfide (−S−S−) compounds tested included glutathione (0.1, 0.3, and 0.5 mM),

cysteine (0.3 mM), and oxidized glutathione (0.3 mM). Typically, 5 mL of test solution in a 10 mL glass beaker was prepared by mixing the thiol or disulfide with $AgNO_3$ in DI water and then subjecting to UV irradiation for 0−24 h. Selected experiments with GSH (1 mM) were conducted in PBS buffer, and a control experiment was carried out using 1 mM $AgNO_3$ in DI water. A high-intensity UV lamp (B-100AP, UVP LLC, CA) was used to provide 365 nm long-wave UV with an average intensity of ~10 mW/cm^2. A glass cover was used to prevent water evaporation, and the UV intensity was measured each time before experiment using a UVX radiometer (UVP LLC, CA) to guarantee the consistency of the irradiation intensity.

Ag-NP formation was also examined in collagen solution and in a collagen gel matrix. Collagen working solutions were prepared by diluting vendor's stock with DI water to 0.1 mg/mL, and the resulting solution was acidic with pH of 3.9 (Orion 8165BNWP electrode, Thermo Scientific), then 1 M NaOH was used to adjust pH to 7.4, and $AgNO_3$ was added to the collagen solutions at 1 mM, followed by UV irradiation (365 nm, ~10 mW/cm^2). Selected experiments were carried out in the dark or ambient lab light. The progress of photodecomposition was monitored by tracking the decrease of soluble Ag^+ concentration using AA after removal of particulate phase with centrifugal ultrafiltration. Selected experiments were conducted in collagen gel matrix to better reflect the physical state of tissue. The collagen gel was prepared following vendor's protocol with modification. Typically, collagen stock solution was diluted with DI water to 4 mg/mL, and $AgNO_3$ was added to concentration of 1 mM, then 1 M NaOH was used to adjust pH to 7.4. The viscous mixture was transferred into a 24-well plate with incubation at 37 °C for 1 h, during which period solidified collagen gel was formed. The collagen gel was then incubated in the dark, under the ambient room light, sunlight, or UV lamp for up to 24 h.

Selenium Reactions with Ag^0 and Ag_2S. Reduced selenium species (Se^{x-}, x = 1, 2) were generated *in situ* by reacting Na_2SeO_3 with $NaBH_4$[93] under anaerobic atmosphere in a glovebox (O_2 ~0.1 ppm, Vacuum Atmospheres, CA). Typically, $NaBH_4$ was mixed with Na_2SeO_3 at 5/1 molar ratio in deoxygenated DI water for 30 min. The formation of Ag_2Se on Ag^0 surfaces was first investigated using silver foil (99.9% Ag) of 0.127 mm thickness cut into 4 mm × 4 mm pieces. To remove possible oxide layers, the small foil sections were dipped into 1% HNO_3 for 5 min before use. A piece of silver foil was incubated in 5 mL of *in situ* reduced selenium species ([Se] = 5 mM) for 7 days in the glovebox. Silver foil incubated in DI water was used as control. Se/S exchange reaction was conducted by treating presulfidated silver nanopowder or silver foil with reduced selenium species. A piece of silver foil or silver nanopowder (10 mM) were first sulfidated with 5 mL of 5 mM Na_2S solution for up to 3 days, followed with purification of sulfidation product with DI water wash using centrifugation. The Se/S exchange was achieved by incubating the obtained sulfidated products in reduced selenium ([Se] = 2.5 or 5 mM) for up to 3 days, followed by sample purification.

Sample Characterization. The UV−vis spectra of aqueous samples were recorded on a V-630 spectrophotometer (Jasco, MD) between 300 and 800 nm. The morphology and size of UV-induced Ag-NPs were determined with transmission electron microscopy (TEM) on a Philips EM420 at 120 kV. TEM samples were prepared by placing a drop of purified sample solution on copper grids with a continuous carbon film coating, followed by solvent evaporation at room temperature overnight. The composition and phase of UV irradiation products were identified by X-ray powder diffraction (XRD) spectrometry on a Bruker AXS D8 Avance diffractometer with Cu Kα radiation (λ = 1.5418 Å). To prepare the XRD sample, a mixture solution containing 1 mM $AgNO_3$ and 0.3 mM GSH was exposed under a UV lamp for 3 h; after sample wash with DI water using centrifugal ultrafiltration, the obtained concentrated nanoparticle suspension was added onto a small glass slide and dried overnight in the dark. The Se-tarnished silver foil surface and the products of Se/S exchange reaction were analyzed by XRD after sample purification with DI water washing and by energy-dispersive X-ray spectroscopy (EDS) on a LEO 1530 field-emission scanning electron microscope (FE-SEM) at 20 kV accelerating voltage and 8.5 mm working distance (see Supporting Information). Samples for SEM and EDS were prepared on silicon substrates, and silver sulfide films before/after selenation were placed directly on the conductive tape, both of which meet the requirement of flat surfaces in the ZAF correction method.

Conflict of Interest: The authors declare no competing financial interest.

Acknowledgment. Financial support was provided by NSF Grant ECCS-1057547, and the Superfund Research Program of the National Institute of Environmental Health Sciences, P42ES013660. Although sponsored in part by NIEHS, this work does not necessarily reflect the views of the agency.

Supporting Information Available: ThioGlo-1 fluorescence assay used for quantification of GSH concentration, experimental phenomena of silver−GSH polymer formation over a wide range of GSH concentrations, reaction stoichiometry of silver−GSH polymer formation, TEM image of Ag-NPs produced by UV irradiation of $AgNO_3$/GSH mixture, Ag-NPs produced by UV irradiation of $AgNO_3$/thiol mixture, photographs of $AgNO_3$ in collagen gel matrix after incubated in the dark, exposure under ambient lab light, sunlight, and UV light, and elemental analysis of sulfidation and Se/S exchange reaction products. This material is available free of charge *via* the Internet at http://pubs.acs.org.

REFERENCES AND NOTES

1. Wiesner, M. R.; Lowry, G. V.; Alvarez, P.; Dionysiou, D.; Biswas, P. Assessing the Risks of Manufactured Nanomaterials. *Environ. Sci. Technol.* **2006**, *40*, 4336–4345.
2. Lowry, G. V.; Gregory, K. B.; Apte, S. C.; Lead, J. R. Transformations of Nanomaterials in the Environment. *Environ. Sci. Technol.* **2012**, *46*, 6893–6899.
3. Lin, D.; Tian, X.; Wu, F.; Xing, B. Fate and Transport of Engineered Nanomaterials in the Environment. *J. Environ. Qual.* **2010**, *39*, 1896–1908.
4. Nowack, B.; Ranville, J. F.; Diamond, S.; Gallego-Urrea, J. A.; Metcalfe, C.; Rose, J.; Horne, N.; Koelmans, A. A.; Klaine, S. J. Potential Scenarios for Nanomaterial Release and Subsequent Alteration in the Environment. *Environ. Toxicol. Chem.* **2012**, *31*, 50–59.
5. Liu, J.; Hurt, R. H. Ion Release Kinetics and Particle Persistence in Aqueous Nano-Silver Colloids. *Environ. Sci. Technol.* **2010**, *44*, 2169–2175.
6. Liu, J.; Sonshine, D. A.; Shervani, S.; Hurt, R. H. Controlled Release of Biologically Active Silver from Nanosilver Surfaces. *ACS Nano* **2010**, *4*, 6903–6913.
7. Liu, J.; Pennell, K. G.; Hurt, R. H. Kinetics and Mechanisms of Nanosilver Oxysulfidation. *Environ. Sci. Technol.* **2011**, *45*, 7345–7353.
8. Levard, C.; Reinsch, B. C.; Michel, F. M.; Oumahi, C.; Lowry, G. V.; Brown, G. E. Sulfidation Processes of PVP-Coated Silver Nanoparticles in Aqueous Solution: Impact on Dissolution Rate. *Environ. Sci. Technol.* **2011**, *45*, 5260–5266.
9. Kim, B.; Park, C.; Murayama, M.; Hochella, M. F. Discovery and Characterization of Silver Sulfide Nanoparticles in Final Sewage Sludge Products. *Environ. Sci. Technol.* **2010**, *44*, 7509–7514.
10. Kaegi, R.; Voegelin, A.; Sinnet, B.; Zuleeg, S.; Hagendorfer, H.; Burkhardt, M.; Siegrist, H. Behavior of Metallic Silver Nanoparticles in a Pilot Wastewater Treatment Plant. *Environ. Sci. Technol.* **2011**, *45*, 3902–3908.
11. Zook, J. M.; Long, S. E.; Cleveland, D.; Geronimo, C. L. A.; MacCuspie, R. I. Measuring Silver Nanoparticle Dissolution in Complex Biological and Environmental Matrices Using UV−Visible Absorbance. *Anal. Bioanal. Chem.* **2011**, *401*, 1993–2002.
12. Kent, R. D.; Vikesland, P. J. Controlled Evaluation of Silver Nanoparticle Dissolution Using Atomic Force Microscopy. *Environ. Sci. Technol.* **2012**, *46*, 6977–6984.
13. Lowry, G. V.; Espinasse, B. P.; Badireddy, A. R.; Richardson, C. J.; Reinsch, B. C.; Bryant, L. D.; Bone, A. J.; Deonarine, A.; Chae, S.; Therezien, M.; *et al.* Long-Term Transformation and

Fate of Manufactured Ag Nanoparticles in a Simulated Large Scale Freshwater Emergent Wetland. *Environ. Sci. Technol.* **2012**, *46*, 7027–7036.
14. Li, X.; Lenhart, J. J. Aggregation and Dissolution of Silver Nanoparticles in Natural Surface Water. *Environ. Sci. Technol.* **2012**, *46*, 5378–5386.
15. Chinnapongse, S. L.; MacCuspie, R. I.; Hackley, V. A. Persistence of Singly Dispersed Silver Nanoparticles in Natural Freshwaters, Synthetic Seawater, and Simulated Estuarine Waters. *Sci. Total Environ.* **2011**, *409*, 2443–2450.
16. Gao, J.; Powers, K.; Wang, Y.; Zhou, H.; Roberts, S. M.; Moudgil, B. M.; Koopman, B.; Barber, D. S. Influence of Suwannee River Humic Acid on Particle Properties and Toxicity of Silver Nanoparticles. *Chemosphere* **2012**, *89*, 96–101.
17. Li, X.; Lenhart, J. J.; Walker, H. W. Dissolution-Accompanied Aggregation Kinetics of Silver Nanoparticles. *Langmuir* **2010**, *26*, 16690–16698.
18. Ma, R.; Levard, C.; Marinakos, S. M.; Cheng, Y.; Liu, J.; Michel, F. M.; Brown, G. E.; Lowry, G. V. Size-Controlled Dissolution of Organic-Coated Silver Nanoparticles. *Environ. Sci. Technol.* **2012**, *46*, 752–759.
19. Zhang, W.; Yao, Y.; Sullivan, N.; Chen, Y. Modeling the Primary Size Effects of Citrate-Coated Silver Nanoparticles on Their Ion Release Kinetics. *Environ. Sci. Technol.* **2011**, *45*, 4422–4428.
20. Huynh, K. A.; Chen, K. L. Aggregation Kinetics of Citrate and Polyvinylpyrrolidone Coated Silver Nanoparticles in Monovalent and Divalent Electrolyte Solutions. *Environ. Sci. Technol.* **2011**, *45*, 5564–5571.
21. Ravindran, A.; Singh, A.; Raichur, A. M.; Chandrasekaran, N.; Mukherjee, A. Studies on Interaction of Colloidal Ag Nanoparticles with Bovine Serum Albumin (BSA). *Colloids Surf., B* **2010**, *76*, 32–37.
22. Khan, S. S.; Srivatsan, P.; Vaishnavi, N.; Mukherjee, A.; Chandrasekaran, N. Interaction of Silver Nanoparticles (SNPs) with Bacterial Extracellular Proteins (ECPs) and Its Adsorption Isotherms and Kinetics. *J. Hazard. Mater.* **2011**, *192*, 299–306.
23. El Badawy, A. M.; Luxton, T. P.; Silva, R. G.; Scheckel, K. G.; Suidan, M. T.; Tolaymat, T. M. Impact of Environmental Conditions (pH, Ionic Strength, and Electrolyte Type) on the Surface Charge and Aggregation of Silver Nanoparticles Suspensions. *Environ. Sci. Technol.* **2010**, *44*, 1260–1266.
24. Xiu, Z.; Ma, J.; Alvarez, P. J. J. Differential Effect of Common Ligands and Molecular Oxygen on Antimicrobial Activity of Silver Nanoparticles *versus* Silver Ions. *Environ. Sci. Technol.* **2011**, *45*, 9003–9008.
25. Reinsch, B. C.; Levard, C.; Li, Z.; Ma, R.; Wise, A.; Gregory, K. B.; Brown, G. E.; Lowry, G. V. Sulfidation of Silver Nanoparticles Decreases *Escherichia coli* Growth Inhibition. *Environ. Sci. Technol.* **2012**, *46*, 6992–7000.
26. Kittler, S.; Greulich, C.; Diendorf, J.; Koller, M.; Epple, M. Toxicity of Silver Nanoparticles Increases during Storage Because of Slow Dissolution under Release of Silver Ions. *Chem. Mater.* **2010**, *22*, 4548–4554.
27. Xiu, Z.; Zhang, Q.; Puppala, H. L.; Colvin, V. L.; Alvarez, P. J. Negligible Particle-Specific Antibacterial Activity of Silver Nanoparticles. *Nano Lett.* **2012**, *12*, 4271–4275.
28. Levard, C.; Hotze, E. M.; Lowry, G. V.; Brown, G. E. Environmental Transformations of Silver Nanoparticles: Impact on Stability and Toxicity. *Environ. Sci. Technol.* **2012**, *46*, 6900–6914.
29. Wiesner, M. R.; Lowry, G. V.; Casman, E.; Bertsch, P. M.; Matson, C. W.; Di Giulio, R. T.; Liu, J.; Hochella, M. F. Meditations on the Ubiquity and Mutability of Nano-Sized Materials in the Environment. *ACS Nano* **2011**, *5*, 8466–8470.
30. Bury, N. R.; Wood, C. M. Mechanism of Branchial Apical Silver Uptake by Rainbow Trout Is *via* the Proton-Coupled Na^+ Channel. *Am. J. Physiol.* **1999**, *277*, R1385–R1391.
31. Solioz, M.; Odermatt, A. Copper and Silver Transport by CopB-ATPase in Membrane Vesicles of *Enterococcus hirae*. *J. Biol. Chem.* **1995**, *270*, 9217–9221.
32. Rogers, K. R.; Bradham, K.; Tolaymat, T.; Thomas, D. J.; Hartmann, T.; Ma, L.; Williams, A. Alterations in Physical State of Silver Nanoparticles Exposed to Synthetic Human Stomach Fluid. *Sci. Total Environ.* **2012**, *420*, 334–339.
33. Aaseth, J.; Olsen, A.; Halse, J.; Hovig, T. Argyria—Tissue Deposition of Silver as Selenide. *Scand. J. Clin. Lab Invest.* **1981**, *41*, 247–251.
34. Sato, S.; Sueki, H.; Nishijima, A. Two Unusual Cases of Argyria: The Application of an Improved Tissue Processing Method for X-ray Microanalysis of Selenium and Sulphur in Silver-Laden Granules. *Br. J. Dermatol.* **1999**, *140*, 158–163.
35. Fisher, N. M.; Marsh, E.; Lazova, R. Scar-Localized Argyria Secondary to Silver Sulfadiazine Cream. *J. Am. Acad. Dermatol.* **2003**, *49*, 730–732.
36. White, J. M. L.; Powell, A. M.; Brady, K.; Russell-Jones, R. Severe Generalized Argyria Secondary to Ingestion of Colloidal Silver Protein. *Clin. Exp. Dermatol.* **2003**, *28*, 254–256.
37. Tomi, N. S.; Kranke, B.; Aberer, W. A Silver Man. *Lancet* **2004**, *363*, p532.
38. Brandt, D.; Park, B.; Hoang, M.; Jacobe, H. T. Argyria Secondary to Ingestion of Homemade Silver Solution. *J. Am. Acad. Dermatol.* **2005**, *53*, S105–S107.
39. Trop, M.; Novak, M.; Rodl, S.; Hellbom, B.; Kroell, W.; Goessler, W. Silver Coated Dressing Acticoat Caused Raised Liver Enzymes and Argyria-like Symptoms in Burn Patient. *J. Traumatol.* **2006**, *60*, 648–652.
40. Vlachou, E.; Chipp, E.; Shale, E.; Wilson, Y. T.; Papini, R.; Moiemen, N. S. The Safety of Nanocrystalline Silver Dressings on Burns: A Study of Systemic Silver Absorption. *Burns* **2007**, *33*, 979–985.
41. Naqvi, A. H.; Shields, J. W.; Abraham, J. L. Nasal Argyria (Deposition of Silver-Selenium) in the Photographic Film Industry: Histopathology and Microanalysis. *Am. J. Otolaryngol.* **2007**, *28*, 430–432.
42. Kim, Y.; Suh, H. S.; Cha, H. J.; Kim, S. H.; Jeong, K. S.; Kim, D. H. A Case of Generalized Argyria after Ingestion of Colloidal Silver Solution. *Am. J. Ind. Med.* **2009**, *52*, 246–250.
43. Chung, I. S.; Lee, M. Y.; Shin, D. H.; Jung, H. R. Three Systemic Argyria Cases after Ingestion of Colloidal Silver Solution. *Int. J. Dermatol.* **2010**, *49*, 1175–1177.
44. Bowden, L. P.; Royer, M. C.; Hallman, J. R.; Lewin-Smith, M.; Lupton, G. P. Rapid Onset of Argyria Induced by a Silver-Containing Dietary Supplement. *J. Cutaneous Pathol.* **2011**, *38*, 832–835.
45. Venclíková, Z.; Benada, O.; Joska, L. Monitoring of Selenium in Oral Cavity Argyria—A Clinical and Microscopic Study. *Neuro. Endocrinol. Lett.* **2011**, *32*, 286–291.
46. Jonas, L.; Bloch, C.; Zimmermann, R.; Stadie, V.; Gross, G. E.; Schäd, S. G. Detection of Silver Sulfide Deposits in the Skin of Patients with Argyria after Long-Term Use of Silver-Containing Drugs. *Ultrastruct. Pathol.* **2007**, *31*, 379–384.
47. Loeschner, K.; Hadrup, N.; Qvortrup, K.; Larsen, A.; Gao, X.; Vogel, U.; Mortensen, A.; Lam, H. R.; Larsen, E. H. Distribution of Silver in Rats Following 28 Days of Repeated Oral Exposure to Silver Nanoparticles or Silver Acetate. *Part. Fibre Toxicol.* **2011**, *8*, 18.
48. Wijnhoven, S. W. P.; Peijnenburg, W. J. G. M.; Herberts, C. A.; Hagens, W. I.; Oomen, A. G.; Heugens, E. H. W.; Roszek, B.; Bisschops, J.; Gosens, I.; Van De Meent, D.; *et al.* Nano-Silver—A Review of Available Date and Knowledge Gaps in Human and Environmental Risk Assessment. *Nanotoxicology* **2009**, *3*, 109–138.
49. Thio, B. J. R.; Montes, M. O.; Mahmoud, M. A.; Lee, D.; Zhou, D.; Keller, A. A. Mobility of Capped Silver Nanoparticles under Environmentally Relevant Conditions. *Environ. Sci. Technol.* **2012**, *46*, 6985–6991.
50. Stebounova, L. V.; Guio, E.; Grassian, V. H. Silver Nanoparticles in Simulated Biological Media: A Study of Aggregation, Sedimentation, and Dissolution. *J. Nanopart. Res.* **2011**, *13*, 233–244.

51. Choi, O.; Hu, Z. Size Dependent and Reactive Oxygen Species Related Nanosilver Toxicity to Nitrifying Bacteria. *Environ. Sci. Technol.* **2008**, *42*, 4583–4588.
52. Sotiriou, G. A.; Pratsinis, S. E. Antibacterial Activity of Nanosilver Ions and Particles. *Environ. Sci. Technol.* **2010**, *44*, 5649–5654.
53. Yang, X.; Gondikas, A. P.; Marinakos, S. M.; Auffan, M.; Liu, J.; Hsu-Kim, H.; Meyer, J. N. Mechanism of Silver Nanoparticle Toxicity Is Dependent on Dissolved Silver and Surface Coating in *Caenorhabditis elegans*. *Environ. Sci. Technol.* **2012**, *46*, 1119–1127.
54. Marques, M. R. C.; Loebenberg, R.; Almukainzi, M. Simulated Biological Fluids with Possible Application in Dissolution Testing. *Dissolution Technol.* **2011**, *18*, 15–28.
55. Trombetta, E. S.; Ebersold, M.; Garrett, W.; Pypaert, M.; Mellman, I. Activation of Lysosomal Function during Dendritic Cell Maturation. *Science* **2003**, *299*, 1400–1403.
56. Schneider, L. A.; Korber, A.; Grabbe, S.; Dissemond, J. Influence of pH on Wound-Healing: A New Perspective for Wound-Therapy? *Arch. Dermatol. Res.* **2007**, *298*, 413–420.
57. Thompson, W. G. Duration of Gastric Digestion of Different Foods. In *Practical Dietetics, with Special Reference to Diet in Disease*, 1st ed.; Appleton and Company: New York, 1903; pp 346−348.
58. Slavin, W.; Carnrick, G. R.; Manning, D. C. Chloride Interferences in Graphite-Furnace Atomic-Absorption Spectrometry. *Anal. Chem.* **1984**, *56*, 163–168.
59. Espinoza, M. G.; Hinks, M. L.; Mendoza, A. M.; Pullman, D. P.; Peterson, K. I. Kinetics of Halide-Induced Decomposition and Aggregation of Silver Nanoparticles. *J. Phys. Chem. C* **2012**, *116*, 8305–8313.
60. Jensen, T. R.; Malinsky, M. D.; Haynes, C. L.; Van Duyne, R. P. Nanosphere Lithography: Tunable Localized Surface Plasmon Resonance Spectra of Silver Nanoparticles. *J. Phys. Chem. B* **2000**, *104*, 10549–10556.
61. Song, J. Y.; Kim, B. S. Rapid Biological Synthesis of Silver Nanoparticles Using Plant Leaf Extracts. *Bioprocess Biosyst. Eng.* **2009**, *32*, 79–84.
62. Zhao, X.; Liu, R.; Teng, Y.; Liu, X. The Interaction between Ag^+ and Bovine Serum Albumin: A Spectroscopic Investigation. *Sci. Total Environ.* **2011**, *409*, 892–897.
63. Lin, S.; Chen, K.; Liang, R. Design and Evaluation of Drug-Loaded Wound Dressing Having Thermo Responsive, Adhesive, Absorptive and Easy Peeling Properties. *Biomaterials* **2001**, *22*, 2999–3004.
64. Iizaka, S.; Sanada, H.; Minematsu, T.; Oba, M.; Nakagami, G.; Koyanagi, H.; Nagase, T.; Konya, C.; Sugama, J. Do Nutritional Markers in Wound Fluid Reflect Pressure Ulcer Status? *Wound Repair Regener.* **2010**, *18*, 31–37.
65. Solubility Product Constants. In *CRC Handbook of Chemistry and Physics*, 91st ed. (Internet version); Haynes, W. M., Ed.; CRC Press/Taylor and Francis: Boca Raton, FL, 2011; pp 8−120.
66. Gustafsson., J. P. *Visual MINTEQ version 3.0: A Chemical Equilibrium Speciation Code*; Department of Land and Water Resources Engineering, KTH, Sweden, 2010.
67. Hogstrand, C.; Wood, C. M. Toward a Better Understanding of the Bioavailability, Physiology and Toxicity of Silver in Fish: Implications for Water Quality Criteria. *Environ. Toxicol. Chem.* **1998**, *17*, 547–561.
68. AshaRani, P. V.; Mun, G. L. K.; Hande, M. P.; Valiyaveettil, S. Cytotoxicity and Genotoxicity of Silver Nanoparticles in Human Cells. *ACS Nano* **2009**, *3*, 279–290.
69. Poon, V. K. M.; Burd, A. *In Vitro* Cytotoxity of Silver: Implication for Clinical Wound Care. *Burns* **2004**, *30*, 140–147.
70. Luoma, S. N. *Silver Nanotechnologies and the Environment: Old Problems or New Challenges*? Woodrow Wilson International Center for Scholars: Washington, DC, 2008.
71. Lansdown, A. B. G. A Pharmacological and Toxicological Profile of Silver as an Antimicrobial Agent in Medical Devices. *Adv. Pharmacol. Sci.* **2010**, *2010*, 910686.
72. Bal, W.; Christodoulou, J.; Sadler, P. J.; Tucker, A. Multi-Metal Binding Site of Serum Albumin. *J. Inorg. Biochem.* **1998**, *70*, 33–39.
73. Laussac, J. P.; Sarkar, B. Characterization of the Copper(II)- and Nickel(II)-Transport Site of Human Serum Albumin. Studies of Copper(II) and Nickel(II) Binding to Peptide 1−24 of Human Serum Albumin by ^{13}C and ^{1}H NMR Spectroscopy. *Biochemistry* **1984**, *23*, 2832–2838.
74. Masuoka, J.; Hegenauer, J.; Van Dyke, B. R.; Saltman, P. Intrinsic Stoichiometric Equilibrium Constants for the Binding of Zinc(II) and Copper(II) to the High Affinity Site of Serum Albumin. *J. Biol. Chem.* **1993**, *268*, 21533–21537.
75. Bar-Or, D.; Lau, E.; Winkler, J. V. A Novel Assay for Cobalt-Albumin Binding and Its Potential as a Marker for Myocardial Ischemia—A Preliminary Report. *J. Emerg. Med.* **2000**, *19*, 311–315.
76. Sugio, S.; Kashima, A.; Mochizuki, S.; Noda, M.; Kobayashi, K. Crystal Structure of Human Serum Albumin at 2.5 Å Resolution. *Protein Eng.* **1999**, *12*, 439–446.
77. Shen, X.; Liang, H.; Guo, J.; Song, C.; He, X.; Yuan, Y. Studies on the Interaction between Ag^+ and Human Serum Albumin. *J. Inorg. Biochem.* **2003**, *95*, 124–130.
78. Adams, N. W. H.; Kramer, J. R. Potentiometric Determination of Silver Thiolate Formation Constants Using a Ag_2S Electrode. *Aquat. Geochem.* **1999**, *5*, 1–11.
79. Ballatori, N. Glutathione Mercaptides as Transport Forms of Metals. *Adv. Pharmacol.* **1994**, *27*, 271–298.
80. Richie, J. P.; Skowronski, L.; Abraham, P.; Leutzinger, Y. Blood Glutathione Concentrations in a Large-Scale Human Study. *Clin. Chem.* **1996**, *42*, 64–70.
81. Odriozola, I.; Ormategui, N.; Loinaz, I.; Pomposo, J. A.; Grande, H. J. Coinage Metal−Glutathione Thiolates as a New Class of Supramolecular Hydrogelators. *Macromol. Symp.* **2008**, *266*, 96–100.
82. Liu, Y.; Ma, W.; Liu, W.; Li, C.; Liu, Y.; Jiang, X.; Tang, Z. Silver(I)−Glutathione Biocoordination Polymer Hydrogel: Effective Antibacterial Activity and Improved Cytocompatibility. *J. Mater. Chem.* **2011**, *21*, 19214–19218.
83. Cecil, R. The Quantitative Reactions of Thiols and Disulphides with Silver Nitrate. *Biochem. J.* **1950**, *47*, 572–584.
84. Bellina, B.; Compagnon, I.; Bertorelle, F.; Broyer, M.; Antoine, R.; Dugourd, P.; Gell, L.; Kulesza, A.; Mitrić, R.; Bonačić-Koutecký, V. Structural and Optical Properties of Isolated Noble Metal-Glutathione Complexes: Insight into the Chemistry of Liganded Nanoclusters. *J. Phys. Chem. C* **2011**, *115*, 24549–24554.
85. Bielmyer, G. K.; Bell, R. A.; Klaine, S. J. Effects of Ligand-Bound Silver on *Ceriodaphnia dubia*. *Environ. Toxicol. Chem.* **2002**, *21*, 2204–2208.
86. Tsipouras, N.; Rix, C. J.; Brady, P. H. Passage of Silver Ions through Membrane-Mimetic Materials, and Its Relevance to Treatment of Burn Wounds with Silver Sulfadiazine Cream. *Clin. Chem.* **1997**, *43*, 290–301.
87. Bell, R. A.; Kramer, J. R. Structural Chemistry and Geochemistry of Silver−Sulfur Compounds: Critical Review. *Environ. Toxicol. Chem.* **1999**, *18*, 9–22.
88. Gao, X.; Gao, T.; Zhang, L. Solution-Solid Growth of α-Monoclinic Selenium Nanowires at Room Temperature. *J. Mater. Chem.* **2003**, *13*, 6–8.
89. Merril, C. R.; Harrington, M. G. "Ultrasensitive" Silver Stains: Their Use Exemplified in the Study of Normal Human Cerebrospinal Fluid Proteins Separated by Two-Dimensional Electrophoresis. *Clin. Chem.* **1984**, *30*, 1938–1942.
90. Furne, J.; Saeed, A.; Levitt, M. D. Whole Tissue Hydrogen Sulfide Concentrations are Orders of Magnitude Lower than Presently Accepted Values. *Am. J. Physiol.* **2008**, *295*, R1479–R1485.
91. Hughes, M. N.; Centelles, M. N.; Moore, K. P. Making and Working with Hydrogen Sulfide: The Chemistry and Generation of Hydrogen Sulfide *in Vitro* and Its Measurement *in Vivo*: A Review. *Free Radical Biol. Med.* **2009**, *47*, 1346–1353.
92. Lee, W. E.; Drago, F. J. Toner Treatments for Photographic Images To Enhance Image Stability. *J. Imaging Sci. Technol.* **1984**, *10*, 119–126.

93. Björnstedt, M.; Odlander, B.; Kuprin, S.; Claesson, H. E.; Holmgren, A. Selenite Incubated with NADPH and Mammalian Thioredoxin Reductase Yields Selenide, Which Inhibits Lipoxygenase and Changes the Electron Spin Resonance Spectrum of the Active Site Iron. *Biochemistry* **1996**, *35*, 8511–8516.
94. Klayman, D. L.; Griffin, T. S. Reaction of Selenium with Sodium-Borohydride in Protic Solvents—Facile Method for Introduction of Selenium into Organic Molecules. *J. Am. Chem. Soc.* **1973**, *95*, 197–199.
95. Beld, J.; Woycechowsky, K. J.; Hilvert, D. Selenoglutathione: Efficient Oxidative Protein Folding by a Diselenide. *Biochemistry* **2007**, *46*, 5382–5390.
96. Chemical Composition of the Human Body. In *CRC Handbook of Chemistry and Physics*, 91st ed. (Internet version); Haynes, W. M., Ed.; CRC Press/Taylor and Francis: Boca Raton, FL, 2011; pp 7−48.
97. Navarro-Alarcon, M.; Cabrera-Vique, C. Selenium in Food and the Human Body: A Review. *Sci. Total Environ.* **2008**, *400*, 115–141.
98. Jeong, U.; Kim, J. U.; Xia, Y. Monodispersed Spherical Colloids of Se@CdSe: Synthesis and Use as Building Blocks in Fabricating Photonic Crystals. *Nano Lett.* **2005**, *5*, 937–942.
99. Johnston, H. J.; Hutchison, G.; Christensen, F. M.; Peters, S.; Hankin, S.; Stone, V. A Review of the *In Vivo* and *In Vitro* Toxicity of Silver and Gold Particulates: Particle Attributes and Biological Mechanisms Responsible for the Observed Toxicity. *Crit. Rev. Toxicol.* **2010**, *40*, 328–346.
100. Lee, S. M.; Lee, S. H. Generalized Argyria after Habitual Use of $AgNO_3$. *J. Dermatol.* **1994**, *21*, 50–53.
101. Westhofen, M.; Schäfer, H. Generalized Argyrosis in Man: Neurotological, Ultrastructural and X-ray Microanalytical Findings. *Arch. Otorhinolaryngol.* **1986**, *243*, 260–264.
102. van der Zande, M.; Vandebriel, R. J.; Van Doren, E.; Kramer, E.; Rivera, Z. H.; Serrano-Rojero, C. S.; Gremmer, E. R.; Mast, J.; Peters, R. J. B.; Hollman, P. C. H.; Hendriksen, P. J. M.; Marvin, H. J. P.; Peijnenburg, A. A. C. M.; Bouwmeester, H. Distribution, Elimination, and Toxicity of Silver Nanoparticles and Silver Ions in Rats after 28-Day Oral Exposure. *ACS Nano* **2012**, *6*, 7427–7442.
103. Glover, R. D.; Miller, J. M.; Hutchison, J. E. Generation of Metal Nanoparticles from Silver and Copper Objects: Nanoparticle Dynamics on Surfaces and Potential Sources of Nanoparticles in the Environment. *ACS Nano* **2011**, *5*, 8950–8957.
104. Liu, H.; Ye, Y.; Chen, J.; Lin, D.; Jiang, Z.; Liu, Z.; Sun, B.; Yang, L.; Liu, J. *In Situ* Photoreduced Silver Nanoparticles on Cysteine: An Insight into the Origin of Chirality. *Chem.—Eur. J.* **2012**, *18*, 8037–8041.
105. Akaighe, N.; MacCuspie, R. I.; Navarro, D. A.; Aga, D. S.; Banerjee, S.; Sohn, M.; Sharma, V. K. Humic Acid-Induced Silver Nanoparticle Formation under Environmentally Relevant Conditions. *Environ. Sci. Technol.* **2011**, *45*, 3895–3901.
106. Hamel, S. C.; Ellickson, K. M.; Lioy, P. J. The Estimation of the Bioaccessibility of Heavy Metals in Soils Using Artificial Biofluids by Two Novel Methods: Mass-Balance and Soil Recapture. *Sci. Total Environ.* **1999**, *244*, 273–283.
107. Liu, X.; Sen, S.; Liu, J.; Kulaots, I.; Geohegan, D.; Kane, A.; Puretzky, A. A.; Rouleau, C. M.; More, K. L.; Palmore, G. T. R.; *et al.* Antioxidant Deactivation on Graphenic Nanocarbon Surfaces. *Small* **2011**, *7*, 2775–2785.